ELSEVIER

Journal of Hazardous Materials A 63 (1998) 5–24

Journal of Hazardous Materials

On modeling of the evaporation of chemical warfare agents on the ground

Susanne Nyholm Westin [a], Stellan Winter [a,*], Edvard Karlsson [a], Art Hin [b], Fokke Oeseburg [b]

[a] *Defence Research Establishment, Division of NBC Defence, SE-901 82, Umeå, Sweden*
[b] *TNO Prins Maurits Laboratorium, Postbus 45, NL-2280 AA Rijswijk ZH, Netherlands*

Received 16 April 1998; revised 15 June 1998; accepted 15 June 1998

Abstract

A model for evaporation of chemical warfare agents on the ground has been developed. The process of evaporation is described in three steps: (1) the immediate drop enlargement due to impact momentum is modeled using an empirical correlation from technical literature; (2) further enlargement caused by capillary spreading upon the surface and the simultaneous sorption into the substrate, modeled in three dimensions; (3) subsequent drying and redistribution of the sorbed material is described as a one-dimensional (vertical) process. The formulation of the flux in the soil takes into account vapour, liquid, solute, and adsorbed phases. The evaporation from the surface is determined by the vapour concentration at the surface and the conditions in the atmospheric viscous sub-layer close to the droplet spots on the surface. Model results agree with the limited experimental data found in the literature. The model shows a very rapid sorption and redistribution of chemical warfare droplets on sand. This effect gives a rapid decrease of the evaporation, except for a shorter initial period. However, a small residual evaporation exists for a rather long time from liquid, which has penetrated down into the soil.

Keywords: Evaporation; Chemical warfare; Vapour concentration

1. Introduction

Persistent chemical warfare agents (boiling point far exceeding environmental temperature) form a ground contamination of liquid droplets, which evaporate and sorb into

* Corresponding author. Tel.: +46 90 10 66 53; fax: +46 90 10 68 00; e-mail: winter@ume.foa.se

0304-3894/98/$ - see front matter
PII: S0304-3894(98)00174-5

the substrate. The evaporation rate and drying of a droplet patch depend on temperature, initial drop volume, enlargement factor, volatility of the agent, wind, mobility of the agent in the substrate, water content and flux in the substrate, water solubility, chemical reactions, adsorption, etc. The evaporation rate process can mainly be described in the following steps below.

(1) *Processes affecting the size of the wet spot*: the enlargement caused by impact momentum and subsequent capillary spreading upon and into the substrate.

(2) *Atmospheric processes*: air flow field over the wet spot; molecular and turbulent diffusion from the surface; three-dimensional effects due to the size of the wet spot and the concentration profile just above the spot and the height of the viscous sub-layer.

(3) *Processes in the substrate affecting the drying*: capillary diffusion of liquid phases (agent and water); diffusion of vapour phase in the air filled spaces; formation of aqueous solution; convection of aqueous solution; adsorption to soil particles and degradation of the agent.

Various models for prediction of the evaporation of CW agents and pesticides have been suggested over the years [1–10]. According to Winter et al. [11], the models may be subdivided into three categories: (a) empirical models, (b) models based on the theories for evaporation from a free liquid surface, and (c) models including processes in the soil.

Comparative studies show (see Aarnink et al. [4]) that the models give mutually very different results, whichever conditions they are applied to. Also, comparisons with experimental data reveal the same confusion, however, this could be, in part, due to a notorious lack of proper mass balance determinations in the experiments.

It seems that the models always lack a proper description of at least one of the three steps mentioned above. For example, it appears that, in fact, all of the models are deficient in their treatment of the step two, atmospheric processes. The most advanced models use evaporation equations intended for lakes or large pools, where the main resistance to vertical diffusion flux takes place in the turbulent boundary layer, and then simply scale down to droplet size, for which all or most of the resistance emanates from the viscous sublayer. This disregard of three-dimensional size effects results in an underestimation of the evaporative flux, as well as the dependency on the wet spot length scale.

Another example is the treatment of the drying processes, where most models use empirical correlations for the drying curve, adopted to some experimental conditions and substrate material. These models do not apply to conditions that deviate substantially from the conditions during the field- or laboratory tests. One model [7] treats drying in a somewhat more physical manner, but neglects liquid phase mobility in the substrate, resulting in an immediate transition to a steep falling rate drying with a substantial underestimation of evaporation rate.

In this work, based on the literature review [11], we suggest a three-step model: (I) the immediate enlargement due to impact momentum is modeled using an empirical correlation from the technical literature [12]; (II) the further enlargement caused by capillary spreading [13] upon the surface and the simultaneous sorption into the substrate is modeled in three dimensions; (III) the subsequent drying and redistribution of the sorbed material is described as a one-dimensional (vertical) process retaining the surface

area of the wet spot obtained in step II constant. The formulation of the flux in the soil takes into account vapour, liquid, solute and adsorbed phases. The flux from the surface is determined by the vapour concentration at the surface and the hight of the vapour blanket over the spot according to Baines and James [14].

The rationale for the assumptions of this model is discussed in the following sections. The suggested model is also compared with some experimental data from the literature.

2. Mathematical model

2.1. Droplet spreading and sorption

When a droplet strikes the ground, the kinetic energy causes an immediate enlargement of the liquid area on the surface (Fig. 1). Subsequently, the liquid will gradually sorb into the soil as a result of capillary forces. The liquid area also continues to increase as a result of the horizontal component of the capillary forces.

2.1.1. Droplet impact

The immediate enlargement of a droplet (with initial spherical radius, R_o) striking the surface, is modeled by using the Sheller and Bousfield [12] correlation, but corrected for the boundary condition at $u_0 = 0$:

$$\frac{R_e}{R_0} = \left\{ \left(\frac{R_{e,min}}{R_0} \right)^6 + 0.1457 \sqrt{\frac{\rho_c^3 R_0^3 u_0^4}{\mu^2 \gamma}} \right\}^{1/6} \quad (1)$$

where R_e is the radius of the droplet immediately after impact, $R_{e,min}$ (m) is the smallest R_e value corresponding to $u_0 = 0$ (assumed to be 1.61 R_0, corresponding to a contact angle of 60°), u_0 is the impact velocity (m s^{-1}), ρ_c is the liquid density (kg m^{-3}), μ is the dynamic liquid viscosity (kg m^{-1} s^{-1}), and γ is the surface tension (N m^{-1}).

The experiments underlying Eq. (1) showed little variation between various substrate materials with small roughness (0.005 to 0.1 μm). It seems unknown how larger

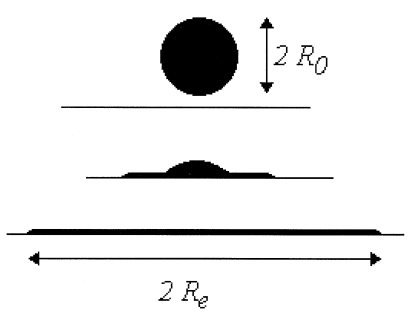

Fig. 1. Example of consecutive shapes of a droplet striking a solid surface. R_0 is the initial radius of the spherical droplet, and R_e is the final spread radius when the kinetic energy has been consumed (based on Fig. 2 in Scheller and Bousfield [12]).

roughness correlates with Eq. (1). However, we suppose that the equation may be used generally.

2.1.2. Spherical cap spreading and capillary sorption

The description of the further motion uses laws for spherical cap spreading and capillary sorption. The cap is supposed to spread according to Eq. (2) (Cazabat and Stuart [13]), and also when the non-sorbed liquid volume V_c (assumed to be shaped as a spherical cap) decreases with time (see Fig. 2):

$$R_c = \left(R_e^{10} + 0.7 V_c^3 \frac{\gamma}{\mu} t \right)^{1/10} \tag{2}$$

To describe the sorption of the liquid into the ground, it is assumed that the vertical distance, x_f, to the center of the wetting front (see Fig. 2) during sorption (i.e. as long as $V_c > 0$) follows the universal laws (the Boltzmann transformation) for one-dimensional sorption (see e.g. Miller and Bresler [15] or Reichhart et al. [16]).

$$x_f = \sigma\sqrt{t} \tag{3}$$

or equivalently

$$\frac{\mathrm{d}x_f}{\mathrm{d}t} = \frac{\sigma^2}{2} \cdot \frac{1}{x_f} \tag{4}$$

where t is the time (s) of sorption. The constant σ is the penetrability (m $s^{-1/2}$), which may be written as the empirical expression [15]:

$$\sigma = \sqrt{\lambda \frac{\gamma}{\mu}} \tag{5}$$

where γ is the liquid surface tension (N m^{-1}), and μ is the liquid viscosity (kg m^{-1} s^{-1}). The constant, λ (m), is a length describing the substrate properties only, and is proportional to the pore sizes.

For the growth of the radius, R, (Fig. 2) caused by horizontal sorption, similar to the vertical sorption, it is assumed that the rate, $\mathrm{d}R/\mathrm{d}t$, is inversely proportional to the

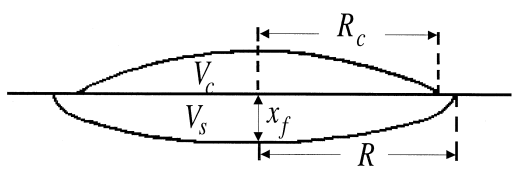

Fig. 2. Sorption into the ground of a spreading droplet with cap volume, V_c (m^3). R_c (m) is the radius of the cap of the liquid droplet on the surface, R (m) is the radius of the liquid sorbed into the porous substrate, and x_f (m) is the distance to the wetting front at the center of the liquid in the substrate (the depth in the substrate). V_s (m^3) denotes the current sorbed volume of liquid, occupying a zone (the lower curve in the figure) in the porous substrate with volume $\beta x_f \pi R^2$ (m^3), see Eq. (7).

distance, $R - R_c$, to the free liquid (the cap) in a similar manner to Eq. (3) or Eq. (4) for the vertical sorption. That means:

$$\frac{dR}{dt} = \frac{\sigma^2}{2} \cdot \frac{1}{R - R_c} \tag{6}$$

In one-dimensional sorption of liquids into soils, it has been found that the mean concentration ($m^3\ m^{-3}$) in the wet layer during sorption is constant $\approx 0.86f$, where f is the effective porosity or the maximum (saturated) concentration ($m^3\ m^{-3}$) [17]. This is also supposed to be the case for the wet zone (height x_f and radius R in Fig. 2) in our three-dimensional problem. Furthermore, it is assumed that the volume of this wetted zone during sorption can be written as, $\beta x_f \pi R^2$, with the constant β slightly smaller than one. In this work, $\beta = 0.80$ has been used, which is, in part, based on ocular observations from experiments.

Hence, the liquid volume, V_s, contained in the wetted zone becomes

$$V_s = (0.86f)\left(\beta x_f \pi R^2\right) \tag{7}$$

Elimination of the liquid cap radius, R_c, in Eq. (6) using the conservation equation (provided that volume loss due to simultaneous evaporation can be neglected), $V_s = (4/3)\pi R_0^3 - V_c$, and Eqs. (2), (3) and (7), give the equation of motion for the radius R of the wet patch during sorption:

$$\frac{dR}{dt} = \frac{\dfrac{\sigma^2}{2}}{R - \left[R_e^{10} + 0.7\left(V_0 - 0.86f\beta\sigma\sqrt{t} \cdot \pi R^2\right)^3 \dfrac{\gamma t}{\mu}\right]^{1/10}}. \tag{8}$$

This equation is solved numerically starting at $R = R_e$ and terminating when $V_c = 0$ ($V_s = V_0$) at $R = R_1$ and $t = t_1$. The penetration depth at the end of spreading–sorption is then, $x_{f1} = \sigma\sqrt{t_1}$.

2.2. Liquid and vapour diffusion in the ground

At the end of sorption, it is supposed that the following drying–redistribution process may be described as a vertical one-dimensional diffusion process. The necessary rearrangements of the three-dimensional geometry are made as follows.

The horizontal radius of the wet spot is assumed not to change during the drying and remains a constant R_1 = the radius at the end of sorption. The wet zone is reshaped into a cylinder, having the radius R_1. The initial depth (the cylinder height) is, H_1 = mean depth of the wetted zone at the end of sorption = $\beta x_{f1} = 0.8\ x_{f1}$ (see Section 2.1.2). In a one-dimensional coordinate system with the positive z-axis pointing upwards and $z = 0$ at the surface, the initial concentration profile is assumed to be

$$\begin{cases} c_t = \rho_c f 0.86 & 0 \geq z \geq -H_1 \\ c_t = 0 & z < -H_1 \end{cases} \tag{9}$$

where $f = \phi - \theta_{w0}$ is the effective porosity, ρ_c is the liquid density of the chemical and c_t is the total concentration of the agent. This choice of initial c_t in the one-dimensional case, is the same as the mean concentration in the wetted area for the sorption process.

2.2.1. Relationship between phases

We assume four one-dimensional transfer processes in the ground: (1) diffusion of vapour phase, (2) capillary diffusion of liquid phase, (3) diffusion of chemical dissolved in soil water, (4) convection of soil water including dissolved chemical. The total agent concentration c_t (kg m^{-3}) is:

$$c_t = \rho_b c_S + \theta_w c_L + a c_g + \eta \rho_c \tag{10}$$

where c_S is the adsorbed concentration (kg kg^{-1}), c_L is the dissolved chemical concentration (kg m^{-3}), c_g is concentration in the vapour phase (kg m^{-3} in soil air), ρ_c is liquid density of the chemical (kg m^{-3}), ρ_b is soil bulk density (kg m^{-3}), θ_w is volumetric water solution content (m^3 m^{-3}), a is air filled porosity (m^3 m^{-3}), and η is liquid chemical concentration (m^3 m^{-3}). The volumetric water solution content is a function of soil porosity, ϕ (m^3 m^{-3}), the air filled porosity, and the liquid chemical concentration:

$$\theta_w = \phi - \eta - a \tag{11}$$

However, the volumetric water solution content, θ_w, also depends on c_L as

$$\theta_w = \theta_{w0} \frac{\rho_w}{\rho_S - c_L} \tag{12}$$

where θ_{w0} is the initial volumetric soil water content (m^3 m^{-3}), ρ_s is the density of the water solution (kg m^{-3}) and ρ_w is liquid density of water (kg m^{-3}).

c_S, c_L, c_g, and η are related to each other through the equilibrium partitioning coefficients or functions:

$$c_g = f(T,\eta)\,\eta \tag{13}$$

$$c_g = K_H c_L \tag{14}$$

$$c_S = K_D c_L \tag{15}$$

where $f(T,\eta)$ in Eq. (13) is a function of temperature T and chemical liquid content η. K_H is Henry's law constant in the non-dimensional form, and K_D (m^3 kg^{-1}) is a linear adsorption coefficient. Based on Mendoza and Frind [18], $f(T,\eta)$ is assumed to be:

$$f(T,\eta) = \begin{cases} \dfrac{c_{gs}}{\eta_{crit}} & 0 < \eta < \eta_{crit} \\ \dfrac{c_{gs}}{\eta} & \eta > \eta_{crit} \end{cases} \tag{16}$$

where η_{crit} (m^3 m^{-3}) is the liquid concentration above which the gas concentration in the pores reaches its saturated value (the volatility), c_{gs} (kg m^{-3}). $\eta_{crit} = 0.01$ is often used [18].

Using Eqs. (10), (13)–(15), c_t can be formulated as:

$$c_t = c_g R_g = \eta R_\eta = c_L R_l \tag{17}$$

where R_g, R_η and R_l are partitioning functions given by:

$$R_g = a + \frac{\rho_c}{f(T,\eta)} + \frac{\theta_w}{K_H} + \frac{\rho_b K_D}{K_H} \tag{18}$$

$$R_\eta = af(T,\eta) + \rho_c + \frac{\theta_w f(T,\eta)}{K_H} + \frac{\rho_b K_D f(T,\eta)}{K_H} \tag{19}$$

$$R_l = aK_H + \frac{K_H \rho_c}{f(T,\eta)} + \theta_w + \rho_b K_D. \tag{20}$$

2.2.2. Diffusion coefficients

To describe the diffusion processes, we use three soil diffusion coefficients, the soil–gas phase diffusion coefficient D_g^s, the soil-dissolved liquid chemical diffusion coefficient D_l^s, and a soil–liquid phase diffusion coefficient D_{lc}^s. The gas phase diffusion coefficient in the substrate is supposed to follow the Millington [19] analysis of the tortuosity factor in partially saturated porous media. According to this theory, the area of pore space exposed in a cut surface is ϕ (m^2 m^{-2}) if ϕ (m^3 m^{-3}) is the total porosity. However, the effective area for transfer depends on the interaction of pores at two different planes, resulting in an effective area which is less than ϕ. Assuming an isotropic porous medium with spherical pores, it can be shown that the effective area is $\phi^{4/3}$. Thus, if only gas or liquid occupies the pores, we obtain $D_g^s/D_g = \phi^{4/3}$ or D_l^s/D_l^{water}. In a similar way, the effect of both gas and liquid can be derived, giving:

$$D_g^s = \frac{a^{10/3}}{\phi^2} D_g \tag{21}$$

$$D_l^s = \frac{\theta_w^{10/3}}{\phi^2} D_l^{water} \tag{22}$$

where D_g is the air–gas diffusion coefficient (m^2 s^{-1}) and D_l^{water} is the diffusion coefficient for the chemical in water. See e.g. Farmer et al. [20], regarding experimental verification of Eqs. (21) and (22).

The description of liquid phase diffusion is more unclear in the literature. However, it is well-established [16,17] that a gradient transport theory using the diffusion coefficient

$$D_l = 1.07 \cdot 10^{-3} \sigma^2 e^{(8.1 \frac{\eta}{\eta_{sat}})} \tag{23}$$

is capable of describing both concentration profiles and fluxes correctly for sorptive processes where $(\partial\eta)/(\partial t) \geq 0$.

In Eq. (23), η is the concentration of liquid chemical (m^3 m^{-3}) and η_{sat} is the maximum possible liquid concentration. In Eq. (23), η_{sat} is approximated with the effective porosity $f = \phi - \theta_{w0}$ in the substrate. σ is the penetrability (m $s^{-1/2}$) as defined in Eqs. (3)–(5).

However, the processes described here are not sorptive but redistributive (sorptive and desorptive simultaneously), with $(\partial\eta)/(\partial t) > 0$ in the lower part of the layer and $(\partial\eta)/(\partial t) < 0$ in the upper part of the layer. Experiments according to Pel et al. [21] show that the form $D \approx D_0 e^{(8.1\eta)/(\eta_{sat})}$ is also applicable in desorptive cases. Furthermore, in an analysis by Philip [22], it is shown that σ in redistributive processes is about $1/3$ of the σ for sorption. Therefore, in this model, we take the liquid phase diffusion coefficient, D^s_{lc}, to be $1/10$ of D_l in Eq. (23):

$$D^s_{lc} = 1.07 \cdot 10^{-4} \cdot \sigma^2 e^{\frac{8.1 \cdot \eta}{\phi - \theta_{w0}}} \tag{24}$$

The reason for this smaller diffusion coefficient for redistribution processes, is a capillary hysteresis phenomenon for sorption and desorption of liquids in porous media, analogous to the equilibrium contact angle hysteresis for liquid fronts advancing or retreating on flat surfaces.

2.2.3. Transport equations in the ground and mass balance

When omitting adsorbed-phase transport, the one-dimensional mass flux equation in the soil can be expressed as:

$$F = -D^s_g \frac{\partial c_g}{\partial z} - D^s_{lc} \frac{\partial(\eta\rho_c)}{\partial z} - D^s_l \frac{\partial c_L}{\partial z} + V c_L \tag{25}$$

where V is the convective velocity of soil water (m s^{-1}) modified for reduced flow area. Eq. (25) can be transformed to:

$$F = -D_1 \frac{\partial c_t}{\partial z} - D_2 c_t \tag{26}$$

where D_1 (m^2 s^{-1}) is an effective diffusion coefficient:

$$D_1 = \frac{D^s_g}{R_g} + \frac{D^s_{lc}\,\rho_c}{R_\eta} + \frac{D^s_l}{R_l} \tag{27}$$

and D_2 (m s^{-1}) corresponds to an effective convection velocity:

$$D_2 = D^s_g \frac{\partial}{\partial z}\left(\frac{1}{R_g}\right) + D^s_{lc}\,\rho_c \frac{\partial}{\partial z}\left(\frac{1}{R_\eta}\right) + D^s_l \frac{\partial}{\partial z}\left(\frac{1}{R_l}\right) - \frac{V}{R_l} \tag{28}$$

The chemical is assumed to undergo a first-order decay in the porous substrate. The mass balance equation is then:

$$\frac{\partial c_t}{\partial t} = -\frac{\partial F}{\partial z} - \varepsilon c_t \tag{29}$$

where ε (s^{-1}) is the first-order degradation coefficient. Using Eq. (26), the mass balance equation is written as a function of D_1 and D_2:

$$\frac{\partial c_t}{\partial t} = \frac{\partial}{\partial z}\left(D_1 \frac{\partial c_t}{\partial z}\right) + \frac{\partial}{\partial z}(D_2 c_t) - \varepsilon c_t. \tag{30}$$

2.2.4. Transport through the ground–air interface (upper boundary condition)

The upper boundary condition is defined by the evaporation flux to the atmosphere and is modeled for individual drop patches according to Baines and James [14]. The evaporation is strongly influenced by two-dimensional internal boundary layers over the drop patches, and the vapour blanket above the patch resides completely in the viscous sublayer where the velocity increases linearly with the vertical distance from the surface. The mean evaporation flux (kg m^{-2} s^{-1}) from the drop patch is:

$$\bar{F} = 0.667 c_{g0} \left(\frac{\kappa D_g^2}{R} \right)^{1/3} \tag{31}$$

where c_{g0} is the vapour concentration (kg m^{-3}) at the surface, R is the radius of the patch (m) (see Fig. (2)), and $\kappa = (du)/(dz) = (u*^2)/(\nu)$ is the velocity shear (s^{-1}) near the surface. $\bar{F}$ may now be expressed in terms of the more familiar friction velocity $u*$ as

$$\bar{F} = 0.667 c_{g0} \left(\frac{D_g^2 u*^2}{\nu R} \right)^{1/3} \tag{32}$$

It should be pointed out that the validity range for the radius, R, in Eq. (32) is limited (up to a few cm), and that the model is not valid for droplet ensembles merging together into larger pools. In that case, a model taking the diffusion in the turbulent boundary layer into account, is needed. Furthermore, the possible effect of a background concentration, c_b, emanating from other droplets upstream, is not considered in Eq. (32). However, this can be introduced by the replacement, $c_{g0} \rightarrow c_{g0} - c_b$. Here, we assume the droplets to be independent of each others and that the evaporation from individual droplets could be added.

2.2.5. Lower boundary conditions

The lower boundary condition for the vertical processes was defined as

$$c_t(z = -\infty, t) = 0 \tag{33}$$

a zero total concentration at an infinite depth at all times.

2.2.6. Numerical methods

Eq. (30) with boundary conditions according to Eqs. (32) and (33), was solved using finite differences with a semi-implicit scheme, similar to Crank–Nicholson's [23]. In each time step, θ_w, ϕ, η, a, c_L, c_g, R_g, R_η, and R_l have to be solved from c_t using the Eqs. (11), (12), (17)–(20) by an iterative process.

3. Model calculation and comparison with experiments

Information about types of substrate, values of experimental variables and model parameters used in model calculations and comparison with experiments are summarized in Table 1.

Table 1
Types of substrate, values of experimental variables, and model parameters used in model calculations and comparison with experiments

Variable	Figs. 3, 5[a], 8	Fig. 4	Fig. 6	Fig. 7
Substrate type	Sand	Concrete	Sand	Sand
R_0 (mm)	0.533	0.533	0.136	0.262
σ (m $s^{-1/2}$)	5.19×10^{-3}	1.18×10^{-4}	5.19×10^{-3}	5.19×10^{-3}
ϕ (m^3 m^{-3})	0.40	–	0.40	0.40
θ_{w0} (m^3 m^{-3})	0.005	–	0.005	0.005
f (m^3 m^{-3})	0.40	0.0832	0.40	0.40
ρ_b (kg m^{-3})	1600	–	1600	1600
K_D (m^3 kg^{-1})	1.665×10^{-5}	–	1.665×10^{-5}	1.665×10^{-5}
η_{crit} (m^3 m^{-3})	0.01	–	0.01	0.01
u_0 (m s^{-1})	4.58 and 0.0	4.58 and 0.0	1.08 and 0.0	2.37 and 0.0
R_e (mm)	1.99[b], 0.858[c]	1.99[b], 0.858[c]	0.248[b], 0.219[c]	0.664[b], 0.422[c]
R_1 (mm)	2.15[b], 1.36[c]	2.65[b], 2.57[c]	0.349[b], 0.335[c]	0.800[b], 0.657[c]
t_1 (s)	0.00094[b], 0.0066[c]	18.5[b], 21.0[c]	0.00037[b], 0.00043[c]	0.00069[b], 0.0017[c]
x_{f1} (mm)	0.159[b], 0.420[c]	0.505[b], 0.534[c]	0.0994[b], 0.108[c]	0.136[b], 0.211[c]
H_1 (mm)	0.127[b], 0.336[c]	0.404[b], 0.427[c]	0.0796[b], 0.0862[c]	0.109[b], 0.169[c]
Initial $\bar{F}$ (g m^{-2} s^{-1})	0.0299[b], 0.0348[c]	–	0.0548[b], 0.0556[c]	0.0416[b], 0.0444[c]

[a]For $u_0 = 4.58$ m s^{-1} only.
[b]For $u_0 > 0$.
[c]For $u_0 = 0$.
All cases are for methyl salicylate at 27°C with the following values mention below.
$\gamma = 0.039$ N m^{-1}.
$\mu = 0.0029$ N s m^{-2}.
$c_{gs} = 1.571\times10^{-3}$ kg m^{-3}.
$\rho_c = 1184$ kg m^{-3}.
$D_g = 8.17\times10^{-6}$ m^2 s^{-1}.
$D_l^{water} = 7.6\times10^{-10}$ m^2 s^{-1}.
$K_H = 1.367\times10^{-3}$, $V = 0$ m s^{-1}.
$\varepsilon = 0$ s^{-1}.
$\nu = 1.5\times10^{-5}$ m^2 s^{-1}.
$u* = 0.106$ m s^{-1}.

3.1. Droplet spreading model

Fig. 3 shows the horizontal radius R_e (1.99 mm and 0.86 mm, respectively, at time nought) after impact and the subsequent radial growth due to capillary spreading and sorption. The calculation is performed for a low viscous droplet with initial spherical radius, $R_0 = 533$ μm, on fine sand ($\lambda = 2.0$ μm) at impact velocities, $u_0 = 4.58$ m s^{-1} (curve A) and 0 m s^{-1} (curve B), respectively.

The time, t_1, for the sorption to be completed is 0.94 ms and 6.6 ms, respectively. The final radius R_1, reached at this time, is 2.15 mm and 1.36 mm, respectively. The corresponding final depth of penetration (at center), $x_{f1} = \sigma\sqrt{t_1}$, is 0.16 mm and 0.42 mm, respectively.

The immediate enlargement of the droplet radius at time zero, is caused by the kinetic energy of the falling droplets (Eq. (1)). The following enlargement of the droplets, until

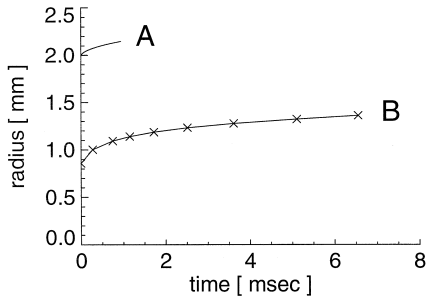

Fig. 3. Radial growth of spreading–sorbing low viscous droplets ($\mu = 0.0029$ N s m^{-2}, $\gamma = 0.039$ N m^{-1}) with $R_0 = 533$ μm, after impact onto a highly sorptive substrate ($f = 0.4$ m^3 m^{-3}, $\lambda = 2.0$ μm, $\sigma = 5.19 \times 10^{-3}$ m s$^{-1/2}$). (A) Droplet after impact with terminal velocity, $u_0 = 4.58$ m s^{-1}. (B) Droplet without ($u_0 = 0$) impact velocity. Data are representative for methyl salicylate at 27°C on fine sand (see Table 1 for further property data).

all liquid is sorbed into the sand, takes place in a very short time due to the high penetrability σ of this liquid-substrate combination. This explains the small further growth ($R_e \rightarrow R_1$) of the horizontal radius in Fig. 3.

However, on other surfaces with smaller σ-values, for example concrete, the processes for droplet enlargement and sorption into the substrate take much longer time. Fig. 4 illustrates the radial growth of droplets with similar liquid properties, impact velocities ($u_0 = 4.58$ m s^{-1} and 0 m s^{-1}) and size as in Fig. 3. This means that the impact radii ($R_e = 1.99$ mm and 0.86 mm) are the same as in the Fig. 3 example. The penetrability σ is, on the other hand, considerably smaller than in Fig. 3, causing a much slower vertical sorption ($t_1 = 18.5$ s and 21.0 s, respectively), allowing for the horizontal growth of the spherical cap (see Section 2) to last a longer time (notice the different time scales in Figs. 3 and 4). This results in a larger total horizontal growth ($R_e \rightarrow R_1$) with a final radius $R_1 = 2.65$ mm and 2.57 mm, respectively. This small difference is also a result of the slow vertical sorption, allowing for the two radii to

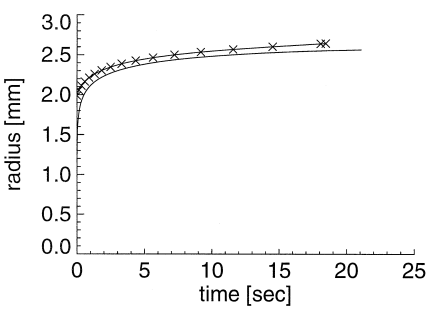

Fig. 4. Radial growth of spreading–sorbing low viscous droplets ($\mu = 0.0029$ N s m^{-2}, $\gamma = 0.039$ N m^{-1}) with $R_0 = 533$ μm, after impact onto a low sorptive substrate ($f = 0.0832$ m^3 m^{-3}, $\lambda = 1.03 \times 10^{-9}$ m, $\sigma = 1.18 \times 10^{-4}$ m s$^{-1/2}$). (×) Droplet after impact with terminal velocity, $u_0 = 4.58$ m s^{-1}. (————) Droplet without ($u_0 = 0$) impact velocity. Data are representative for methyl salicylate at 27°C on dry concrete.

catch up with each other, despite the large initial difference in R_e. The substrate properties, f and λ, (see caption, Fig. 4) are based on measurements with acetone and a type of concrete [24].

3.2. Liquid and vapour diffusion in the ground

Fig. 5 shows a calculated example for the time development of the vertical concentration profile in the substrate, following the sorption–spreading as described by the curve A in Fig. 3 (initial spherical radius is 533 μm).

The substrate and liquid properties are the same as in Fig. 3 and Table 1. The initial depth, H_1, of the wet zone is 0.127 mm ($= 0.8 \times 0.159$ mm). The initial mean flux from the surface is $\bar{F} = 3.0 \times 10^{-5}$ kg m^{-2} s^{-1}, corresponding to a volatility, $c_{gs} = c_{g0} = 1.571 \times 10^{-3}$ kg m^{-3}, gas phase diffusion coefficient, $D_g = 8.17 \times 10^{-6}$ m^2 s^{-1}, friction velocity $u* = 0.106$ m s^{-1}, and air viscosity $\nu = 1.5 \times 10^{-5}$ m^2 s^{-1}.

3.3. Comparison with experimental data

In the literature, there are some experiments dealing with evaporation of droplets on the ground. However, it is difficult to use this data for comparisons with the present

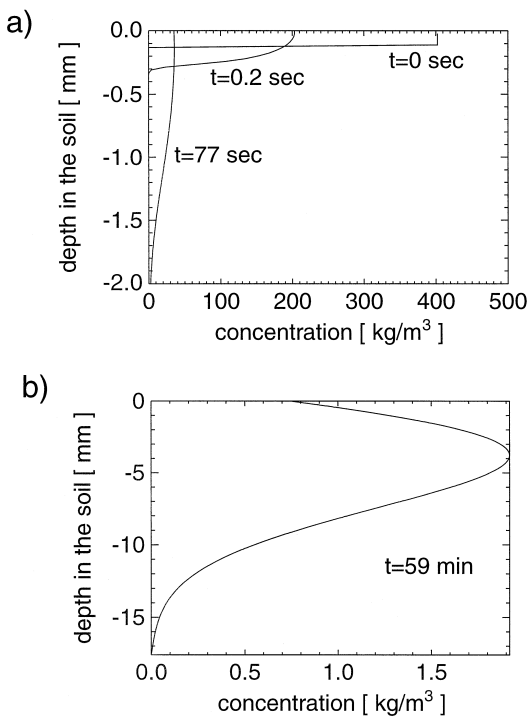

Fig. 5. Time development of the vertical concentration profile in the substrate following the sorption–spreading as described by the curve A in Fig. 3. (a) After 0 s, 0.2 s, and 77 s. (b) After 59 min. The radius, R_1,of the wet spot is 2.15 mm and the initial (mean) evaporative flux from the surface is $\bar{F} = 3.0 \times 10^{-5}$ kg m^{-2} s^{-1}. Further substrate and liquid properties may be found in Table 1.

model because the input data is missing or is inadequately measured. Information on droplet impingement speed and sorptive properties of the substrate is always very meager. Data allowing for an estimate of the air flow near the surface (i.e. $u*$ or corresponding) are also often inadequate.

There are a few experiments, where the uncertainties in the model input are at a reasonable level. Reichman et al. [25] reports on the evaporation of methyl salicylate droplets from three different soils, using a wind tunnel with a rectangular (width 42 cm, height 3–10 cm) cross-section at the evaporating surface. The evaporation rate was determined by measuring the concentration (Miran 1A spectrophotometer) at the tunnel outlet together with the volume flow rate through the tunnel.

Only the tests on dune sand (100% quartz sand) allowed for a reasonable estimate of the friction velocity, $u*$. Using information about the mean flow speed ($\bar{u} = 1.6$ m s^{-1}) in the test section together with graphs showing tunnel outlet concentration and residual quantity, it was possible to estimate that the volume flow rate through the tunnel was in the range ≈ 0.023–0.024 m^3 s^{-1} for the droplet sizes tested. This gives a wind tunnel height, $H \approx 0.035$ m. Using a correlation [26] for an infinitely wide channel with equilibrium flow

$$\frac{\bar{u}}{u*} = 2.5 \ln\left[\frac{1.66 u* H}{\nu}\right] \tag{34}$$

the friction velocity was estimated to be $u* = 0.106$ m s^{-1}, using $\nu = 1.5 \times 10^{-5}$ m^2 s^{-1} for the air kinematic viscosity. The size of the wet spots were not recorded in the experiments.

The experimental temperature was stated to be 24–30°C and the physical properties of methyl salicylate, used in the model calculations, were estimated at 27°C as: $\gamma = 0.039$ N m^{-1}, $\mu = 0.0029$ N s m^{-2} (measured in our laboratory), $\rho_c = 1184$ kg m^{-3}, $c_{gs} = 1.571 \times 10^{-3}$ kg m^{-3}, $D_g = 8.17 \times 10^{-6}$ m^2 s^{-1}, $K_H = 1.367 \times 10^{-3}$, $D_l^{water} = 7.6 \times 10^{-10}$ m^2 s^{-1}.

The dune sand had a bulk density, $\rho_b = 1600$ kg m^{-3} with a porosity, $\phi = 0.40$, and a water content, $\theta_{w0} = 0.005$ m^3 m^{-3}. The liquid sorption properties of the sand were not stated in the article by Reichman et al. [25], but penetrability data for various sand types can be found in the soil science literature. It seems that penetrabilities in the range $\sigma = 10$–15 mm s$^{-1/2}$ are typical [27] for sorption of water into most sands. This corresponds to a length scale, λ, (Eq. (5)), in the range 1.4–3 μm. In the present model calculations we use $\lambda = 2.0$ μm.

Regarding the combined chemical-substrate properties, the hygroscopic limit concentration (see Section 2.2.1), η_{crit}, was set equal to 0.01 and the linear adsorption coefficient, K_D, was estimated to be 1.665×10^{-5} m^3 kg^{-1} [9]. The liquid penetrability was calculated (Eq. (5)) as $\sigma = 0.00519$ m s$^{-1/2}$.

Figs. 6–8 show comparisons between these experiments and the present model results for methyl salicylate droplets with three different drop sizes ($R_0 = 136$, 262, and 533 μm). Note the two-level variation of the impact speed, u_0, in the model results. The impact velocities in the experiments are completely unknown, therefore, model calculations were performed using both $u_0 = 0$ and $u_0 =$ full terminal settling velocity for the three drop sizes. The evaporation is presented in the form of Q_{tot}/M_{tot} (s^{-1}) as a

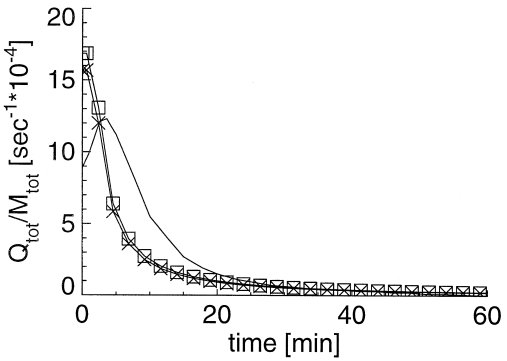

Fig. 6. Comparison between experiment, (————) and model (□, ×) of the evaporation of methyl salicylate droplets ($R_0 = 136$ μm) from dune sand at 27°C. (□) Terminal impact velocity, $u_0 = 1.08$ m s^{-1}, $R_e = 248$ μm, $R_1 = 349$ μm and initial flux $\bar{F} = 5.48 \times 10^{-5}$ kg m^{-2} s^{-1}. (X) For $u_0 = 0$, $R_e = 219$ μm, $R_1 = 335$ μm and initial flux $\bar{F} = 5.56 \times 10^{-5}$ kg m^{-2} s^{-1}.

function of time. $Q_{tot} = \bar{F}\pi R_1^2$ is the total evaporation rate (kg s^{-1}), where R_1 is the radius of the evaporating spot and $\bar{F}$ is the average flux from the surface (Eq. (32)). $M_{tot} = (4/3)\pi R_0^3 \rho_c$ is the total initial mass. The initial Q_{tot}/M_{tot} (the plateau) in the model curves is the same as for a free liquid surface; i.e., the surface concentration c_{g0} in Eq. (32) for $\bar{F}$ is the volatility c_{gs}.

The Miran photometer (chamber volume: 5.6 l, volumetric flow rate: 10 l min^{-1}) causes a time delay and smoothing in the experimental concentration–time curves. The dissemination of the droplets might also contribute in a similar manner. This explains at least part of the initial evaporation rise seen in Figs. 6–8.

Fig. 6 shows Q_{tot}/M_{tot} as a function of time for the smallest droplet, $R_0 = 133$ μm, with model impact velocities, $u_0 = 0$ m s^{-1} and 1.08 m s^{-1}. The two curves for the

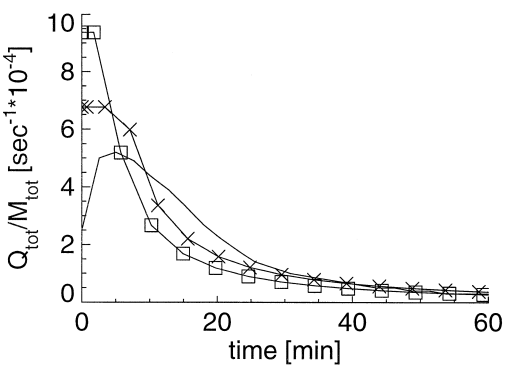

Fig. 7. Comparison between experiment, (————) and model (□, ×) of the evaporation of methyl salicylate droplets ($R_0 = 262$ μm) from dune sand at 27°C. (□) Terminal impact velocity, $u_0 = 2.37$ m s^{-1}, $R_e = 664$ μm, $R_1 = 800$ μm and initial flux $\bar{F} = 4.16 \times 10^{-5}$ kg m^{-2} s^{-1}. (X) For $u_0 = 0$, $R_e = 422$ μm, $R_1 = 657$ μm and initial flux $\bar{F} = 4.44 \times 10^{-5}$ kg m^{-2} s^{-1}.

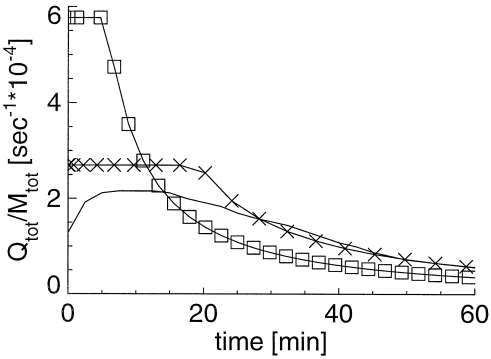

Fig. 8. Comparison between experiment, (————) and model (□, ×) of the evaporation of methyl salicylate droplets ($R_0 = 533$ μm) from dune sand at 27°C. (□) Terminal impact velocity, $u_0 = 4.58$ m s^{-1}, $R_e = 1988$ μm, $R_1 = 2147$ μm and initial flux $\bar{F} = 2.99 \times 10^{-5}$ kg m^{-2} s^{-1}. (X) For $u_0 = 0$, $R_e = 858$ μm, $R_1 = 1361$ μm and initial flux $\bar{F} = 3.49 \times 10^{-5}$ kg m^{-2} s^{-1}.

different impact velocities are close to each other, because the kinetic energies of the falling droplets are too small to affect them. There is a difference between the model curves and the experimental curve in the beginning of the process (however, see above regarding possible experimental time delays). The model curves coincide with the experimental curve in the time range 20–60 min.

Fig. 7 shows Q_{tot}/M_{tot} as a function of time for the $R_0 = 262$ μm droplet, with impact velocities, $u_0 = 0$ m s^{-1} and 2.37 m s^{-1}. The model curve for $u_0 = 2.37$ m s^{-1} has a higher value for Q_{tot}/M_{tot} than the model curve for $u_0 = 0$ m s^{-1}, which is closer to the experimental curve. This is caused by the different impact velocities. The model curve for $u_0 = 0$ m s^{-1} coincides rather well with the experimental curve, especially in the time range 15–60 min.

Fig. 8 shows Q_{tot}/M_{tot} as a function of time for the biggest droplet at $R_0 = 533$ μm, with impact velocities, $u_0 = 0$ m s^{-1} and 4.58 m s^{-1}. There is a big difference between the experimental curve and the model curve, with $u_0 = 4.58$ m s^{-1}. On the other hand, the model curve with $u_0 = 0$ m s^{-1} fits very well with the experimental curve.

4. Discussion

We have not been able to compare the droplet spreading–sorption submodel directly with experiments. Some experimental investigations gave values on enlargement factors, R_1/R_0, but had little information about important input parameters like impact speed, u_0, and the liquid-substrate penetrability σ. Other experiments (see Section 3), on the other hand, gave some (indirect) indications on the input data, but did not tell about the size, R_1/R_0. The droplet spreading is modeled for porous horizontal surfaces, like sand, soil, concrete, and asphalt. However, the model principle could be extended to e.g., vegetation if the effect of non-horizontal surfaces is incorporated.

The surface evaporation model (Eqs. (31) and (32)) for the mean flux from a circular patch, according to Baines and James [14], is in fact derived as a two-dimensional model

for an infinitely wide strip of length, L (in the wind direction), whereafter it is stated, that a circular patch of radius $R = L/\sqrt{\pi}$ has the same mean flux. Comparisons with experimental results [14] neither verify, nor contradict this flux model, because of the wide scatter in the empirical data. Better controlled experiments are required. This especially applies to the determination of the wind shear $\mathrm{d}u/\mathrm{d}z$ at the surface.

In the one-dimensional ground transport model, no direct formulations of gas phase or chemical liquid phase adsorption on soil particles are given, since these can be derived from Eqs. (13)–(15) as $c_s = (c_g K_D)/(K_H)$ and $c_s = (K_D)/(K_H) f(T,\eta)\eta$. However, at gas concentrations less than the saturation concentration ($c_g < c_{gs}$, $\eta < \eta_{crit}$), $\rho_b c_s$ and $\rho_c \eta$ tend to have the same meaning, since equilibrium is assumed. Thus, to be strictly consistent, $(\rho_b K_D)/(\rho_c K_H) f(T,\eta)$ should approach 1.0. For example, for methyl salicylate, this quantity amounts to 0.01–0.001. When detailed experimental values are available for cases with $c_g < c_{gs}$ and $\eta < \eta_{crit}$, this should be examined and adjusted.

There are other ways of modeling the diffusion coefficients for gas and solute diffusion than Eqs. (21) and (22). For example, Blumberg and Schlünder [28] take into account that mass transfer is possible either by parallel diffusion through pores filled completely with gas or liquid, or serial diffusion through gas- and liquid-filled regions. Therefore, a comparison between different formulations are valuable.

The vertical convection speed (V) of water, will depend on evaporation of water, precipitation and the difference between θ_{w0} and the field capacity of the soil. Thus, if these values are known, V can be determined. The first-order decay of the chemical, assumed in Eq. (29), is probably satisfactory for many agents with fast evaporation. However, for more persistent agents, with an evaporation time of days or longer, a more sophisticated decay description may be needed.

In the total integrated model, the submodel for droplet spreading on the surface and sorption into the soil is formulated as a three-dimensional process until all liquid on the surface (the liquid cap) has sorbed into the substrate. In the subsequent submodel for mass flux in soil (Eq. (25)), horizontal fluxes are neglected, which may result in an oversimplification. However, the vertical transfer is probably the dominating process, at least in the beginning, when the horizontal dimensions are much larger than the vertical dimension. Consequently, the area for diffusion in the horizontal directions is small. Later on, the simplification may become more serious. The comparisons with experimental results do not suggest that this is the case. The reason for this may be that an increased horizontal evaporation area, caused by horizontal diffusion, is associated with a corresponding reduction of the evaporation flux per unit area due to the reduced total chemical concentration.

There were no experiments available to verify the total integrated model. For example, the comparisons in Section 3 deal with a single substrate (dry sand), a single liquid, and a single wind speed. Furthermore, the model penetrability had to be based on investigations with water and similar substrates. The impact speed was unknown and was, therefore, varied between its upper and lower limits. In spite of this, the model and experimental results concur rather well.

We were unable to find any experiments dealing with other substrate types and liquid properties, that are capable of producing useful model input data for comparisons.

Specially designed experiments are necessary, to enable verification of the model for wider range of parameters. In such experiments, all parameters defining the agent, the substrate and the atmosphere should be determined. Furthermore, specific experiments may be necessary to study subprocesses such as:

- The wind profile slope $\mathrm{d}u/\mathrm{d}z$ (or the micrometeorological $u*$) at the evaporating surfaces.
- The liquid sorption properties of the substrate, i.e., the penetrability, σ, or (preferably) the length scale, $\lambda = \sigma^2\mu/\gamma = x_f^2\mu/t\gamma$, which is independent of liquid properties.
- The droplet impact speed and the subsequent horizontal, as well as the vertical spreading of the droplets.

Finally, it is important to note that the model in this work only deals with the evaporation of a single droplet in its local environment. In order to get a more general model for the evaporation of disseminated CW-agents, it is necessary to include inhomogeneities in substrate, air flow, droplet size, etc.

5. Nomenclature

a	Air filled porosity $= \phi - \eta - \theta_w$	$m^3\ m^{-3}$
c_g	Concentration of chemical vapour phase in soil air	$kg\ m^{-3}$
c_{g0}	Vapour concentration at the surface	$kg\ m^{-3}$
c_{gs}	Volatility = saturated vapour concentration	$kg\ m^{-3}$
c_L	Concentration of dissolved chemical in soil water	$kg\ m^{-3}$
c_s	Concentration of adsorbed chemical	$kg\ kg^{-1}$
c_t	Total concentration of chemical in the ground	$kg\ m^{-3}$
D_g	Diffusion coefficient for chemical vapour in air	$m^2\ s^{-1}$
D_g^s	Effective vapour diffusion coefficient in the soil	$m^2\ s^{-1}$
D_l^s	Effective diffusion coefficient for dissolved chemical in the soil	$m^2\ s^{-1}$
D_l^{water}	Diffusion coefficient for chemical in water	$m^2\ s^{-1}$
D_1	Effective diffusion coefficient	$m^2\ s^{-1}$
D_2	Effective convection velocity	$m\ s^{-1}$
D_{lc}^s	Diffusion coefficient for liquid phase chemical in the soil	$m^2\ s^{-1}$
f	Effective porosity of the substrate $= \phi - \theta_{w0}$	$m^3\ m^{-3}$
$f(T,\eta)$	Partitioning function for vapour and liquid phases $= c_g/\eta$	$kg\ m^{-3}$
F	Mass flux of chemical	$kg\ m^{-2}\ s^{-1}$
$\bar{F}$	Mean flux of chemical from the surface	$kg\ m^{-2}\ s^{-1}$
H_1	Mean depth of the wet layer at the end of sorption $= \beta x_{f1}$	m
K_D	Linear adsorption coefficient $= c_s/c_L$	$m^3\ kg^{-1}$
K_H	Non-dimensional Henry's law constant	–
R	Radius of spreading droplet patch	m
R_o	Radius of spherical droplet	m

R_1	Horizontal radius of the wet spot at the end of sorption	m
R_e	The droplet radius after impact	m
$R_{e,min}$	Smallest value of R_e for settling velocity $u_0 = 0$	m
R_g	Partitioning function for total and vapour concentrations $= c_t/c_g$	–
R_c	Horizontal radius of liquid spherical cap	m
R_l	Partitioning function for total and dissolved concentrations $= c_t/c_L$	–
R_η	Partitioning function for total and liquid concentrations $= c_t/\eta$	–
t	Time	s
t_1	Time for sorption to be completed	s
T	Temperature	K
u	Wind velocity	m s^{-1}
u_0	Settling velocity of falling droplet	m s^{-1}
$u*$	Friction velocity	m s^{-1}
V	Convective (vertical) velocity of soil water	m s^{-1}
V_0	Initial volume of the spherical droplet	m^3
V_c	Volume of liquid spherical cap	m^3
V_s	Liquid volume contained in the wetted zone	m^3
x_f	Vertical distance from the soil surface to the wetting front	m
x_{f1}	Depth of wetting front at the end of sorption	m
z	Vertical coordinate	m
β	Coefficient (= 0.8 in this work) defining the volume $(= \beta x_f \pi R^2)$ of the wetted zone	–
ε	Time constant for (first-order) degradation of the chemical in the soil	s^{-1}
γ	Surface tension of liquid chemical	N m^{-1}
η	Liquid chemical concentration	m^3 $(m^3$ soil$)^{-1}$
η_{crit}	Limit for liquid concentration, above which the vapour concentration becomes saturated $(c_g = c_{gs})$	m^3 m^{-3}
η_{sat}	Maximum liquid concentration. Expected to be = f	m^3 m^{-3}
θ_w	Volumetric content of soil water solution	m^3 m^{-3}
θ_{w0}	Volumetric soil water content (before attachment of chemical)	m^3 m^{-3}
κ	Air velocity shear near the surface	s^{-1}
λ	Length scale for porous substrate	m
μ	Dynamic viscosity of liquid chemical	kg m^{-1} s^{-1}
ν	Kinematic viscosity of atmospheric air	m^2 s^{-1}
ρ_b	Soil bulk density	kg m^{-3}
ρ_c	Density of liquid chemical	kg m^{-3}
ρ_w	Liquid density of water	kg m^{-3}
ρ_s	Density of water solution	kg m^{-3}
σ	Penetrability $= x_f/\sqrt{t}$ = constant	m $s^{-1/2}$
ϕ	Total soil porosity	m^3 m^{-3}

Acknowledgements

The authors are very grateful to H. Holmström and E. Näslund for their skillful and patient assistance with various computer programs. The authors are also very indebted to L. Thaning for his helpful discussions.

References

[1] J. Monaghan, W.R. McPherson, A mathematical model for predicting vapour dosages on and downwind of contaminated areas of grassland, Suffield technical paper no. 386, September 1971.
[2] K.S.K. Chinn, A simple method for predicting chemical agent evaporation, DPG-TR-401, U.S. Army Dugway Proving Ground, 1981.
[3] J. Medema, C.J.P. van Buytenen, Calculation of the vapour dosage downwind from a contaminated source, Internal report, Prins Maurits Laboratorium TNO, Rijswijk, Netherlands, 1 January 1986.
[4] W.A.M. Aarnink, R.P. Sterkenburg, C.A. van Beest, A.R.T. Hin, Some models for the evaporation of chemical agents from different substrate types, TNO-report, PML 1993-IN 25, November 1993.
[5] L. Thaning, L. Rittfeldt, M. Nordstrand, Fältförsök med tributylsulfat på grus vid temperaturer omkring 5°C, FOA-R-96-00260-4.6, 1996.
[6] T.G. Richard, in: W.J. Lyman, W.F. Reehl, D.H. Rosenblatt (Eds.), Handbook of Chemical Property Estimation Methods, American Chemical Society, Washington, DC, 1990, pp. 16-25–16-27.
[7] L.D. Roberts, Droplet evaporation from porous surfaces, Report no. 2044-002-CBDE, Porton Down, Salisbury, UK, 1994.
[8] W.A. Jury, W.F. Spencer, W.J. Farmer, Behavior assessment model for tracer organics in soil: I. Model description, J. Environ. Qual. 12 (1983) 558–564.
[9] R. Reichman, R. Wallach, Evaporation of volatile organic chemicals from soils—modeling and experimental results, in: Proceedings of 5th International Symposium Protection Against Chemical and Biological Warfare Agents, Stockholm, Sweden, 11–16 June, 1995, FOA-R-95-00122-4.9-SE, pp. 393–402.
[10] K. Riikonen, J. Nikmo, J. Kukkonen, The extension of a consequence analysis model to include liquid pool vaporisation, Finnish Meteorological Institute, Air Quality Dept., to be published.
[11] S. Winter, E. Karlsson, S. Nyholm, A. Hin, F. Oeseburg, Models for the evaporation of chemical warfare agents and other tracer chemicals on the ground: a literature review, in: Proceedings of the 1966 ERDEC Scientific Conference on Chemical and Biological Defense Research, Aberdeen Proving Ground, Maryland, 19–22 November 1996, ERDEC-SP-048, 1997, pp. 41–48.
[12] B.L. Sheller, D.W. Bousfield, Newtonian drop impact with a solid surface, AIChE Journal 41 (1995) 1357–1367.
[13] A.M. Cazabat, M.A. Stuart, Dynamics of wetting: effects of surface roughness, J. Phys. Chem. 90 (1986) 5845–5849.
[14] W.D. Baines, D.F. James, Evaporation of a droplet on a surface, Ind. Eng. Chem. Res. 33 (1994) 411–416.
[15] R.D. Miller, E. Bresler, A quick method for estimating soil water diffusivity functions, Soil Sci. Soc. Am. J. 41 (1977) 1021–1022.
[16] K. Reichhart, D.R. Nielsen, J.W. Biggar, Scaling of horizontal infiltration into homogeneous soils, Soil Sci. Soc. Am. Proc. 36 (1972) 241–245.
[17] W. Brutsaert, Universal constants for scaling the exponential soil water diffusivity, Water Resour. Res. 15 (1979) 481–483.
[18] C.A. Mendoza, E.O. Frind, Advective–dispersive transport of dense organic vapors in the unsaturated zone: 2. Sensitivity analysis, Water Resour. Res. 26 (1990) 388–398.
[19] R.J. Millington, Gas diffusion in porous media, Science, 130 (159), pp. 100–102
[20] W.J. Farmer, M.S. Yang, J. Letey, W.F. Spencer, Hexachlorobenzene: its vapor pressure and vapor phase diffusion in soil, Soil Sci. Soc. Am. Proc. 44 (1980) 676–680.

[21] L. Pel, A.A.J. Ketelaars, O.C.G. Adan, A.A. van Well, Determination of moisture diffusivity in porous media using scanning neutron radiography, Int. J. Heat Mass Transfer 36 (1993) 1261–1267.
[22] J.R. Philip, Horizontal redistribution with capillary hysteresis, Water Resour. Res. 27 (1991) 1459–1469.
[23] J. Crank, The Mathematics of Diffusion, 2nd edn., Clarendon Press, Oxford, 1975, pp. 144–146.
[24] H.W. Reinhardt, M. Aufrecht, Simultaneous transport of an organic liquid and gas in concrete, Materials and Structures 28 (1995) 43–51.
[25] R. Reichman, E. Eyal, N. Dayan, Y. Mahrer, Laboratory simulation for evaluating the effect of droplet size on pesticide persistence in dry soils, Soil Science 148 (1989) 191–198.
[26] H. Rouse, Elementary Mechanics of Fluids, Dover Publications, New York, 1978, p. 214.
[27] E.G. Youngs, R.I. Price, Scaling of infiltration behaviour in dissimilar porous materials, Water Resour. Res. 17 (1981) 1065–1070.
[28] W. Blumberg, E.-U. Schlünder, Simultaneous vapor and liquid diffusion in partially wetted porous media, Drying technology 11 (1993) 41–64.